

Review

# Photoacoustic Imaging in Oxygen Detection

Fei Cao, Zhihai Qiu, Huanhao Li  and Puxiang Lai \*

Department of Biomedical Engineering, The Hong Kong Polytechnic University, Hong Kong 999077, China; demi.cao@connect.polyu.hk (F.C.); zhihai.p.qiu@connect.polyu.hk (Z.Q.); huanhao.li@connect.polyu.hk (H.L.)

\* Correspondence: puxiang.lai@polyu.edu.hk

Academic Editors: Yuanjin Zheng and Fei Gao

Received: 5 October 2017; Accepted: 30 October 2017; Published: 4 December 2017

**Abstract:** Oxygen level, including blood oxygen saturation ( $sO_2$ ) and tissue oxygen partial pressure ( $pO_2$ ), are crucial physiological parameters in life science. This paper reviews the importance of these two parameters and the detection methods for them, focusing on the application of photoacoustic imaging in this scenario.  $sO_2$  is traditionally detected with optical spectra-based methods, and has recently been proven uniquely efficient by using photoacoustic methods.  $pO_2$ , on the other hand, is typically detected by PET, MRI, or pure optical approaches, yet with limited spatial resolution, imaging frame rate, or penetration depth. Great potential has also been demonstrated by employing photoacoustic imaging to overcome the existing limitations of the aforementioned techniques.

**Keywords:** photoacoustic imaging; oxygen saturation; oxygen partial pressure

## 1. Introduction

Oxygen is one of the most essential substances on the earth, ensuring normal life activities and taking part in important processes in manufacturing and chemical industry. The detection and quantification of oxygen level is critical in all these processes to have accurate control, which ensures production efficiency and product quality, and it is extremely vital in life-related scenarios as well. On the one side, lacking oxygen or failure to quantify oxygen levels precisely in living systems may induce fainting, tissue necrosis, or even death [1]. On the other side, many clinical diseases can cause lack of oxygen supply, which directly affects cell metabolism, resists treatment, worsens conditions, prevents recovery, or even can endanger people's lives if the hypoxic circumstances are not properly handled [1]. Therefore, cancer microenvironments have gained great attention recently for both understanding of cancer biology and improving of therapeutic regimes. With changes in proteins, oxygenation, PH value, etc., cancerous lesions are commonly associated with angiogenesis and metastasis [2]. Among all the parameters, oxygen levels play an essential role; tumor hypoxia has been shown to have a close relationship with the resistance of chemotherapy or radiotherapy [3]. For example, researchers are investigating new treating modalities called hypoxia modification therapy, using hyperbaric oxygen [4] or small-particle oxygen delivery systems [5] to improve tumor oxygen conditions and hence to help prevent tumor expansion and therapy resistance. In other examples like severe traumatic brain injury [6,7], great loss of blood may induce severe cerebral ischemia and harm the brain. In wound healing [8], doctors may need to monitor the changes of the local oxygen levels to prevent tissue necrosis and estimate the healing potential. In biomachining processes, the redox state needs to be precisely controlled for high-quality metal removal by microorganisms [9,10].

As such an important parameter in clinical situations, oxygen levels can be characterized by blood oxygen saturation ( $sO_2$ ) and oxygen partial pressure ( $pO_2$ ) in soft tissue. Oxygen saturation ( $sO_2$ ) is a vital respiration parameter, mainly representing the oxygen in the blood, and can be calculated by the ratio between oxygen-saturated hemoglobin and total hemoglobin in the blood. Real-time monitoring of the arterial blood oxygen saturation is very important in clinical care. Spectral-based methods by

using a fingerstall-style photoelectric sensor to detect the transmission of 660 nm and 940 nm near infrared light have long been used to conveniently measure  $sO_2$  [11]. Comparably, much less attention has been put onto  $pO_2$  under clinical conditions.  $pO_2$  can be used to describe the partial pressure of oxygen within the interstitial space of a particular tissue, representing the balance between local oxygen delivery and consumption at any given time [12]. The concept of  $pO_2$  should be of great importance as well, especially in blood-thinning regions or inside solid tumors, where limited vessels exist to transmit oxygen, or diffusion-limited effects block oxygen transmission into the solid tumors. Compared to  $sO_2$ , much less work has been done in exploring means to noninvasively and directly measure  $pO_2$  of biological tissues thus far.

Photoacoustic imaging (PAI), which enables noninvasive optical contrast sensing with acoustic resolution in deep tissue, has attracted more and more attention in the past two decades [13]. While similar to ultrasound imaging (UI) in many ways, PAI has advantages in two aspects. Technically speaking, since PA signals are excited internally by electromagnetic absorption and propagate one way to the detectors, small speed variations do not much affect the travel time of the sound in a finite-length path. Hence, PAI has better tolerance to sound speed variation than conventional pulse-echo ultrasound imaging which detects round-trip ultrasound [14]. On the application level, the UI signal originates from the acoustic impedance mismatch between different tissues, while the PA signal comes from the preferential light absorption spectra of tissues. Therefore, PAI provides better tissue differentiating capability [15].

Since its development, PAI has been regarded as a scalable imaging tool to help understand life activities from both macroscopic and microscopic fields of view. On a coarse scale, photoacoustic computed tomography (PACT) can image at several-centimeter-depth with an acoustic resolution at a seconds-to-minutes 3D imaging speed. In a fine scale, acoustic-resolution photoacoustic microscope (AR-PAM) can provide up to 10 mm imaging depth with acoustic resolution by focused transducers, which can be on the order of tens of micrometers with a MHz frequency transducer. In the highest resolution regime, optical-resolution photoacoustic microscope (OR-PAM) with tightly focused laser illumination can provide sub-wavelength resolution whilst the imaging depth is within a few hundred micrometers. As oxygen distribution in the body holds great heterogeneity, such as between arteries and veins, among tissues, cells, and even organelles, the adjustable imaging depth and resolution of a single modality can greatly facilitate understanding oxygen uptake and metabolism in different scales and finally drawing a whole picture. In this review, we briefly discuss the application of photoacoustic imaging in both  $sO_2$  and  $pO_2$  detection, including the state-of-the-art as well as their potentials and limitations.

## 2. Photoacoustic Imaging in $sO_2$ Measurement

As discussed, yielding strong optical contrast is one facet in which PAI is superior to UI. The most typical case here is hemoglobin absorption. Hemoglobin, as the most important protein that delivers oxygen from respiratory organs to the rest of the body, can either be bound to oxygen molecules, forming oxyhemoglobin ( $HbO_2$ ), or desaturated with oxygen and form deoxyhemoglobin ( $HbR$ ). These two forms of hemoglobin have different peak absorptions between 500–600 nm wavelength range as well as 700–900 nm wavelength range (Figure 1) and thus can be differentiated using spectral method [16]. The generated heat due to the absorption produces ultrasonic waves that can be acquired by a single or a series of transducers and be used to calculate the oxygen saturation in blood. This has been one of the most important and popular applications of PAI.

Moreover, as can be seen from Figure 1,  $HbO_2$  and  $HbR$  are the two major endogenous absorbers, which provide strong photoacoustic signals for  $sO_2$  measurement. Basically, the blood absorption coefficient  $\mu_a(\lambda_i)$  can be expressed as

$$\mu_a(\lambda_i) = \varepsilon_{HbR}(\lambda_i)[HbR] + \varepsilon_{HbO_2}(\lambda_i)[HbO_2], \quad (1)$$

where  $\epsilon_{HbR}(\lambda_i)$  and  $\epsilon_{HbO_2}(\lambda_i)$  are the molar extinction coefficients ( $\text{cm}^{-1}\text{M}^{-1}$ ) of HbR and HbO<sub>2</sub> at a certain wavelength  $\lambda_i$ , and  $[HbR]$  and  $[HbO_2]$  are the concentrations of them, respectively. Since the strength of photoacoustic signal  $\phi(\lambda_i, x, y, z)$  is proportional to the local illuminated energy deposition,  $\mu_a(\lambda_i)$  in Equation (1) can be replaced by  $\phi(\lambda_i, x, y, z)$  and thus we can calculate and get the two concentrations as follows,

$$\begin{bmatrix} HbR \\ HbO_2 \end{bmatrix}_{(x,y,z)} = (M^T M)^{-1} M^T \phi(x, y, z) K, \tag{2}$$

in which

$$M = \begin{bmatrix} \epsilon_{HbR}(\lambda_1) & \epsilon_{HbO_2}(\lambda_1) \\ \vdots & \vdots \\ \epsilon_{HbR}(\lambda_n) & \epsilon_{HbO_2}(\lambda_n) \end{bmatrix}, \phi(x, y, z) = \begin{bmatrix} \phi(\lambda_1, x, y, z) \\ \vdots \\ \phi(\lambda_n, x, y, z) \end{bmatrix}$$

Here,  $K$  is an unknown coefficient that is influenced by the local optical fluence as light passes through the skin, which is wavelength dependent, and by the different ultrasonic parameters [17]. Thus, the  $sO_2$  can be calculated as

$$sO_{2(x,y,z)} = \frac{[HbO_2]_{(x,y,z)}}{[HbO_2]_{(x,y,z)} + [HbR]_{(x,y,z)}}, \tag{3}$$

Several factors during this process may induce error, reducing measurement accuracy, subsequently increasing uncertainty. These factors include the unknown coefficient  $K$ , number of wavelengths applied during the experiment which will affect the accuracy of least-squares fitting, accuracy of molar extinction coefficients at different wavelengths, and the detection component which is directly related with the signal strength. Zhang et al. investigated the principle of measuring  $sO_2$  by photoacoustic microscopy with using four wavelengths between 500–600 nm range [18] The results were compared with those from optical absorption calculated ones measured by a spectrophotometer in the 700–1000 nm range, and they were agreed with each other with a systematic difference of 4%. In order to improve the precision and the reliability of spectral measurement of blood oxygen saturation, Li et al. [19] found that a specific wavelength combination of 660 nm and 805 nm responded more significantly to the changes in blood  $sO_2$ , and can detect  $sO_2$  between 88–100% range. This makes it capable of detecting mixed and venous  $sO_2$  and to some extent superior to traditional oximetry [20] that using 750 nm and 850 nm, which is mostly used to measure arterial  $sO_2$ .

Unlike conventional spectral-based methods that give only oxygen saturation levels, PAI can yield simultaneous 3D imaging information including anatomical, functional, histological, and metabolic parameters. For example, together with vascular diameter and blood flow, PAI is a unique technique for measuring metabolic rate of oxygen (MRO<sub>2</sub>), which is helpful for fundamental pathophysiological studies, and even early diagnosis and treatment of diseases. By using a high-frequency ultrasonic transducer with a large bandwidth and high numerical aperture, the detected acoustic waves can be reconstructed and be localized into a very small volume with high spatial resolution to give information about the optical absorption distribution inside small samples. Specifically, under the condition that the illumination and ultrasonic focal volumes assembled well confocally, a PAM system is capable of providing a signal-to-background contrast of 3500% with high sensitivity and specificity in vivo [21]. With a single small-vessel-resolution photoacoustic microscopy (PAM) system, Yao et al. [22] calculated the metabolism rate of oxygen as well as its changes with environmental thermal conditions, and for the first time obtained five quantitative parameters simultaneously. As shown in Figure 2a, hemodynamic responses to a hyperthermic challenge (red bars) and the relative changes of the skin temperature, vessel diameter, total hemoglobin concentration,  $sO_2$ , blood flow speed, oxygen extraction fraction (OEF), and metabolic rate of oxygen (MRO<sub>2</sub>) are measured by PAM. It must be noted, however, these parameters in the aforementioned study were measured in different spatial scales, which affected the resolution of imaging MRO<sub>2</sub>. Later on,

Ning et al. [23] simultaneously quantified microvascular diameter, oxygen saturation of hemoglobin, and blood flow at the same spatial scale and improved the resolution down to a capillary level in vivo. As can be seen from Figure 2b, Simultaneous PAM of these factors (from i to iii) and their dynamic changes (from iv to vi) revealed by vessel segmentations are shown. Apart from resolution, fast imaging speed is also pursued to capture the blood oxygenation process, which reflects the acceleration of  $sO_2$  change. For example, Yao et al. [24] developed a high-speed functional PAM system for mouse brain imaging, and demonstrated capillary-level-resolution blood oxygenation with a one-dimensional imaging rate of 100 kHz. As shown in Figure 2c, the left hindlimb of a mouse is electrically stimulated,  $sO_2$  in different conditions are imaged, and fractional changes in the cerebral blood flow (CBF), oxygen extraction fraction (OEF), and cerebral metabolic rate of oxygen ( $CMRO_2$ ) in the core responding region are quickly recorded. Emelianov et al. [25] trialed dynamic hemoglobin oxygenation in a pregnant mouse using spectral photoacoustic imaging, which is the first step towards functional imaging of the maternal-fetal environment (Figure 2d).

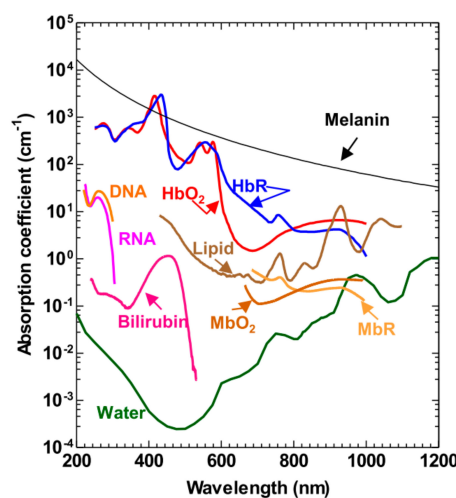


**Figure 1.** Absorption spectra of major endogenous contrast agents in biological tissue at normal concentrations (reproduced with permission from [16]. Copyright Elsevier, 2014).

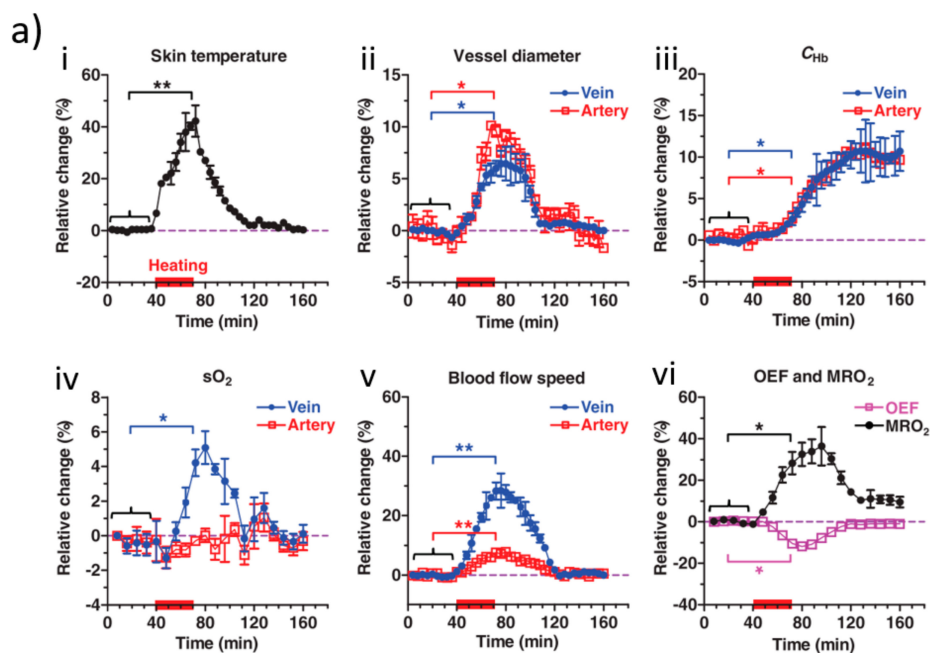


**Figure 2.** Cont.

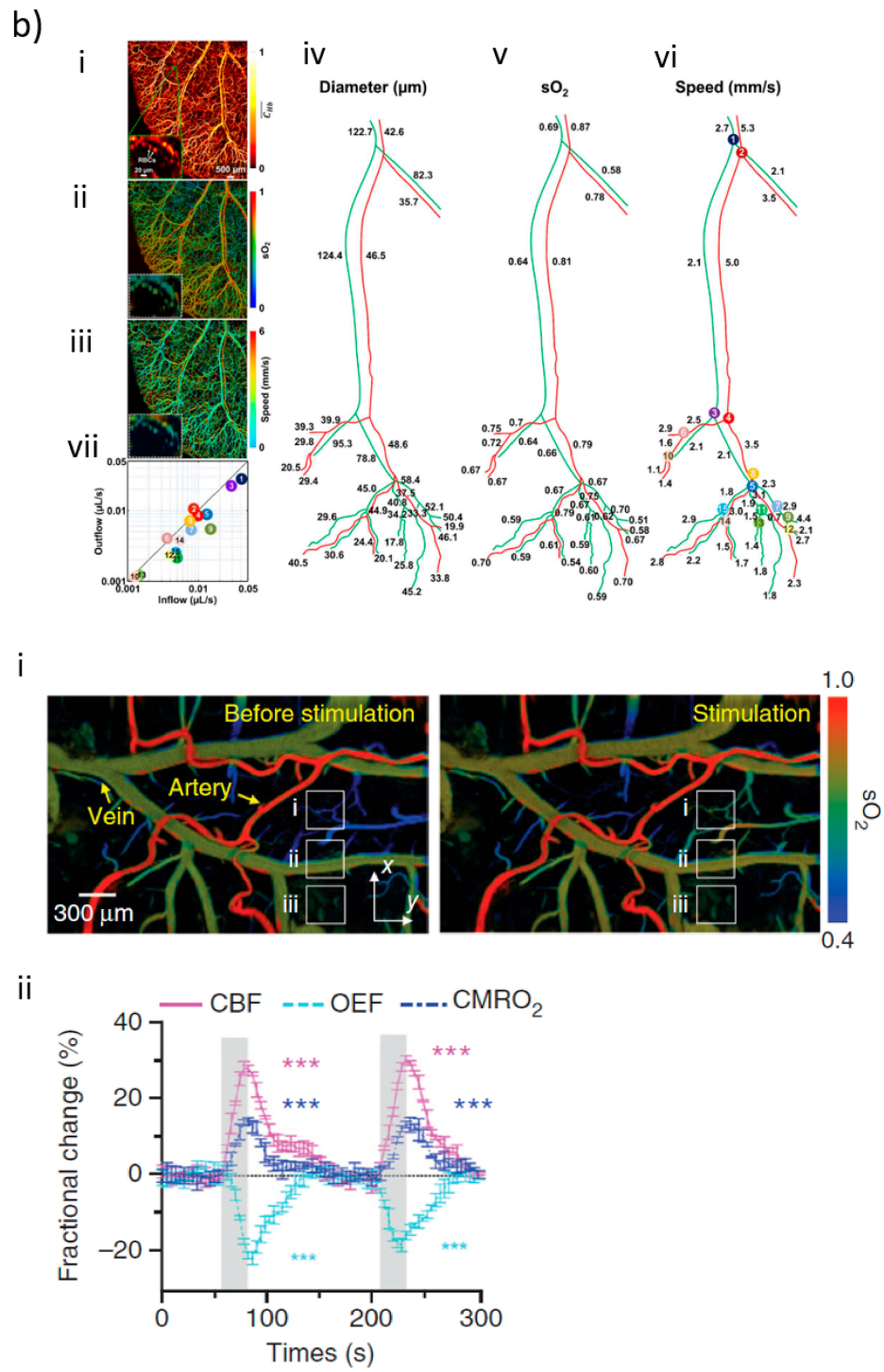
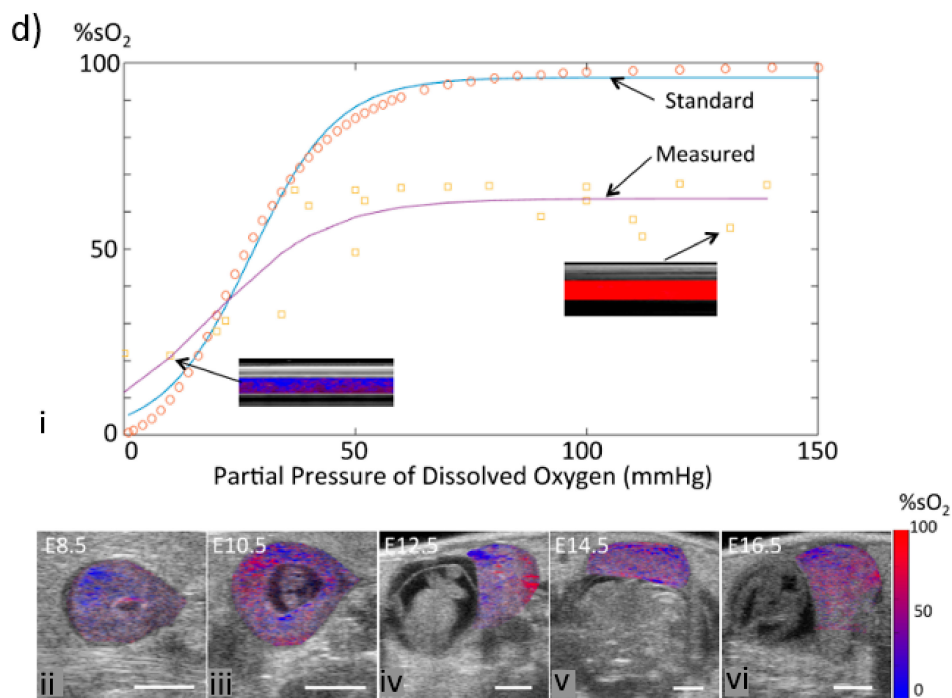


Figure 2. Cont.



**Figure 2.** (a) PAM measurement of hemodynamic responses to a hyperthermic challenge (red bars) and the relative changes (reproduced with permission from [22]. Copyright SPIE, 2011). (b) Simultaneous PAM of (i) vascular anatomy; (ii) oxygen saturation of hemoglobin ( $sO_2$ ); and (iii) blood flow speed in a nude mouse ear in vivo and their dynamics (reproduced with permission from [23]. Copyright The Optical Society, 2015). (c) Quantification of mouse brain oxygenation responses to electrical stimulations (reproduced with permission from [24]. Copyright Nature Publishing Group, 2015). (d) Longitudinal in vivo imaging of regional tissue  $sO_2$  during development (reproduced with permission from [25]. Copyright The Optical Society, 2017).

Not only as a reflection of blood-oxygen supply,  $sO_2$  is also used to infer tissue oxygen condition in most of the work done with PAI. The hypothesis is that  $pO_2$  of tissue has a close relationship with  $sO_2$  in blood, and  $pO_2$  may increase with increased oxygen delivery and decrease with insufficient blood oxygen [26]. That said,  $sO_2$  reflects oxygen supply and delivery, but does not reflect the oxygen consumption in tissue, thus yielding an inaccurate estimation of oxygen level inside soft tissue. On the other side, theoretical analysis also shows that although the tissue oxygenation is deterministically related to vascular oxygenation, the relationship between them is not unequivocal, as variability exists among the fractions of values below the sensitivity thresholds of various measurement methods which in turn could be reflected in the power of correlations between results from different methods or in the selection of patients for prognostic studies [27]. Increasing demand for the accurate monitoring of tissue oxygen levels makes it an urgent need to detect  $pO_2$  parameters directly.

### 3. Photoacoustic Imaging in $pO_2$ Measurement

So far, clinical  $pO_2$  monitoring mainly rely on the oxygen polarographic needle (Eppendorf<sup>®</sup> electrode), positron emission tomography (PET), or magnetic resonance imaging (MRI) based methods. As an invasive approach, Eppendorf<sup>®</sup> electrode has been used since 1993 [28], which contributes to most of the current knowledge about tissue hypoxia. The clinical used PET [29,30] concentrates more on oxygen metabolism, i.e., the glycolysis (F-18-fluorodeoxyglucose (FDG) as an in vivo glycolytic marker which reflects the alterations of glucose metabolism in cancer cells). PET has super sensitivity and good temporal resolution, but poor spatial resolution. PET cannot differentiate two isotopes that are injected simultaneously, as they give two  $\gamma$ -rays with the same energy. In addition,

PET imaging cannot be exploited for too long time or with frequency because of its radiative nature. MRI techniques for oxygen sensing rely on the probes containing the elements of  $^{19}\text{F}$  or  $^1\text{H}$  [31], which are not radioactive and less expensive than PET. MRI techniques can give finer spatial resolution, which is very favored to obtain more detailed anatomical images. However, MRI typically has a low imaging speed, which limits its applications in time-resolved imaging scenarios [32]. Moreover, relying on magnetic fields, this method is not suitable for patients who wear magnetic metal devices or cardiac pacemakers; the generated heat and the big noise during the measuring process may make patients feel uncomfortable and harm them [33]. Therefore, none of the aforementioned methods can be used as a routine tool for noninvasive, high temporal and spatial resolution, and low-cost human tissue oxygen sensing. The biggest concern in tissue  $\text{pO}_2$  imaging may come from its huge heterogeneity [34]. Till now, neither PET nor MRI can completely provide simultaneous temporal and spatial real-time monitoring of tissue oxygen levels.

Optical methods have played more and more important roles in biomedicine, and has the ability to present high temporal and spatial resolution [35]. Methods for biological oxygen partial pressure sensing are mostly through a luminescence quenching way, which images the lifetime of an oxygen-sensitive dye. Luminescence quenching method was proposed in 1935 [36], then first implemented in 1987 [37], and has been the major method used in biological-oxygen-related studies. In luminescence-based methods, phosphorescence and delayed fluorescence quenching are the two major mechanisms. Figure 3a shows that the delayed fluorescence (green and dashed) and phosphorescence (orange) related to triplet state lifetime are most commonly used. Collision between ambient oxygen and triplet-state molecules provides basic principle of this method, in which energy transfer leads to decreased triplet-state population and thus shortens the lifetime of this state. In Figure 3b [38], how the lifetime systems normally works is briefly shown. The general time window for an image is given by the integration time of the camera that turns the camera into a ready-to-accept-light state. Within this time frame, a structure of events if repeated at a defined repetition frequency, for example, for image window 1: the excitation light is switched on and off, consequently the luminescence follows with a certain delay in rise and decay, for image window 1 the camera is 'opened' by the modulation signal for a time  $\Delta_i$ . This sequence is repeated. For image window 2 and the window 'dark', the delays after switching off the excitation light are different but the width  $\Delta_i$  is the same. Different from intensity-based imaging, molecular lifetime is a relatively stable parameter in certain ambient environments, and can elude effects of dye concentration, heterogeneous distribution, and light scattering in tissue. This relatively 'intrinsic' property of lifetime imaging makes it a strong candidate for imaging tissue oxygen condition, and is considered sufficiently sensitive to produce high-contrast spatial heterogeneous information of tissue oxygenation [39,40]. In addition, quenching method is a reversible way, in which the upper state lifetime or the luminescence intensity of the oxygen-sensitive dye is reduced with high oxygen concentration, but can be recovered with low oxygen concentration. Therefore, the quenching method opens a new avenue to accomplish real-time recording of the change of  $\text{pO}_2$ , and hence has gained great development in recent years. The representative fluorescence lifetime microscopy (FLIM) (Figure 3c [41]) has especially contributed a lot in today's *in vitro* trials. As can be seen from Figure 3c, the system employs a pulsed laser whose beam is focused into a spot which is scanned across the sample, dedicated timing electronics, and a single point detector. Nevertheless, optical lifetime microscopes, similar to traditional optical methods, are incapable of yielding fine spatial resolution and deep penetration depth in tissue simultaneously due to the strong scattering of light in tissue.

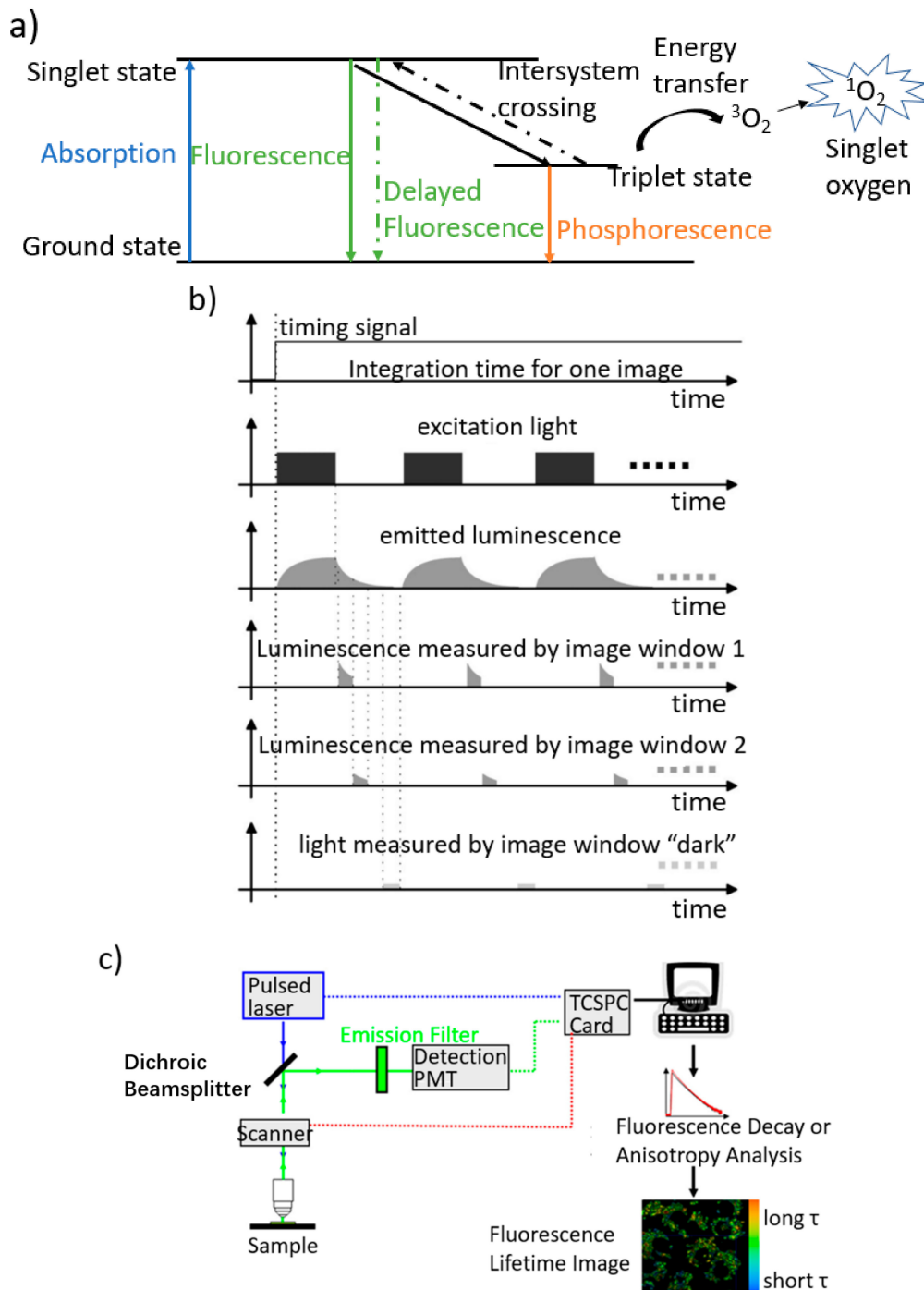


**Figure 3.** (a) Jablonski diagram for oxygen sensing mechanisms; (b) Structure of timing and light signals (reproduced with permission from [38]. Copyright Elsevier, 2001); (c) A schematic time-correlated single photon counting (TCSPC)-based scanning FLIM set-up (reproduced with permission from [41]. Copyright Elsevier, 2015).

Recently there has been a trend to combine photoacoustic imaging with traditional optical imaging mechanisms to obtain deep tissue information. For example, photoacoustic lifetime imaging (PALI) utilizes photoacoustic technique for probing the lifetime of fluorophore’s excited state (Figure 4a) [42]. In optical lifetime microscopies, a pulse wave is first applied to excite the molecules from the ground state to the upper state. Then a time gating method or TCSPC (time correlated single photon counting) scheme is used to record the fluorescence decay from the singlet state or phosphorescence decay

from the triplet state in the time domain, or use phase modulation to get the signal in the frequency domain. By contrast, PALI detects the population of the molecules at the upper state by absorption. In a typical PALI system, as shown in Figure 4a, the measurement of an object requires two lasers. The first pulse (pump) is for excitation, which pumps the molecules to the excited triplet state where transient absorption happens. The transient absorption is then probed by a second laser to generate the photoacoustic waves from triplet–triplet absorption, of which the signal is closely related to the molecule population of the triplet state. Time delay between the pump and probe pulses are tuned to capture the time-dependent photoacoustic amplitude. The higher the  $pO_2$  in the surrounding environment, the faster the excited triplet state population decreases, and hence the faster PA amplitude reduces. By changing the delay between the pump and probe laser pulses, the luminescence decay can be detected, and finally be fit into an exponential function to compute the lifetime.

This principle was first proposed by Shai Ashkenazi et al. [43,44], who have also conducted further studies with methylene blue (MB) solution to demonstrate this concept and pushed it to in vivo. They have built a multi-modal system integrating ultrasound imaging, regular photoacoustic imaging, as well as PALI (Figure 4b) to map the distribution of oxygen partial pressure in tissue, from which hypoxic areas can be clearly identified [45,46]. Based on these studies, they further developed treatment/imaging modality referred to as PDT-PALI (Figure 4c), which enables real-time feedback of three essential parameters during a PDT therapy: tissue oxygen, light penetration in tumor location, and distribution of photosensitizer [47,48]. Lifetime-based PAT technique by using G2 molecules for blood oxygenation sensing [49,50] and MB loaded polyacrylamide nanoparticles (MB-PAA NPs) for tumor oxygen sensing [51] have also been demonstrated by other groups.

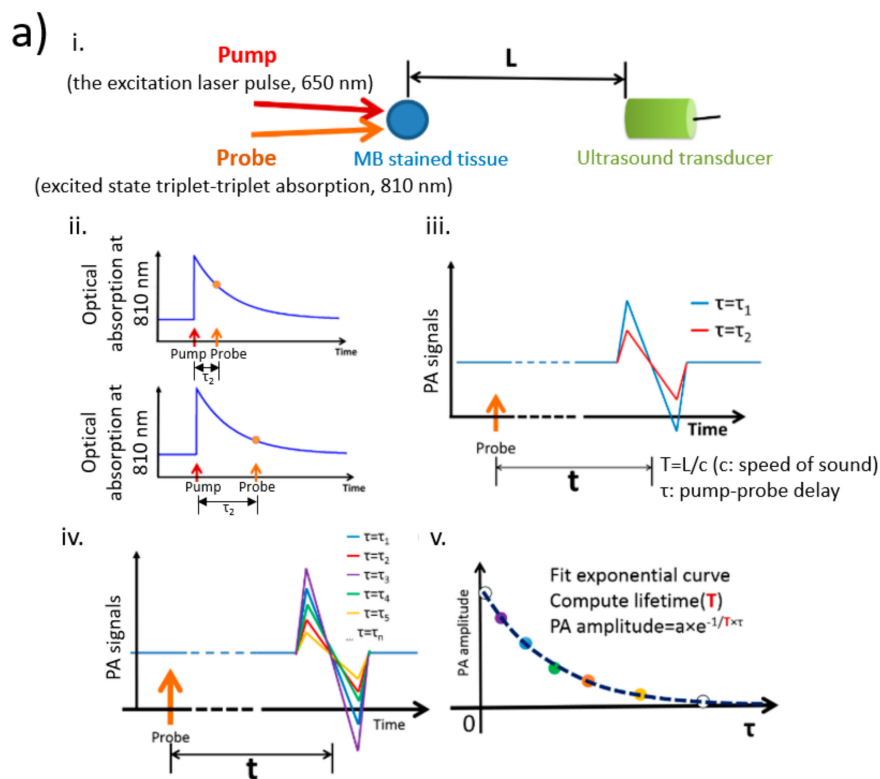
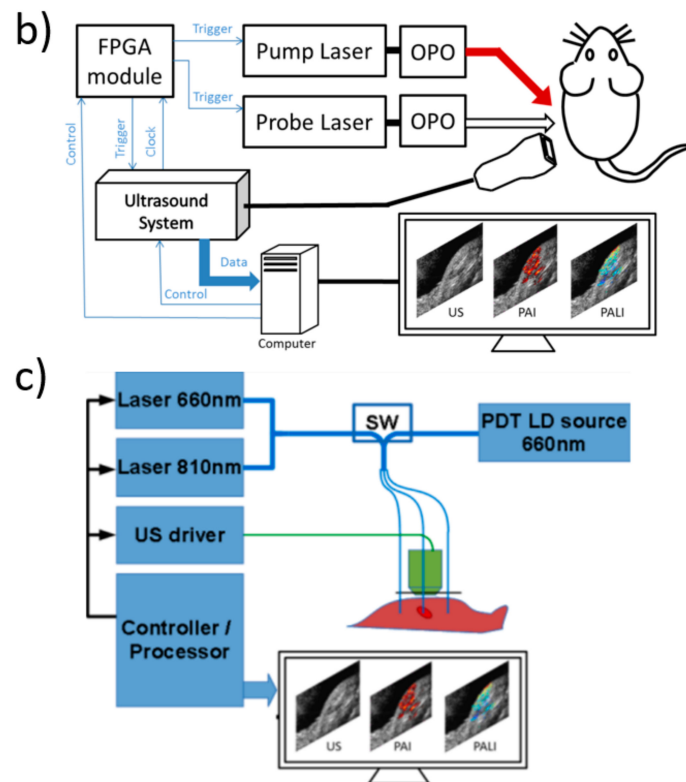


Figure 4. Cont.



**Figure 4.** (a) Photoacoustic lifetime imaging for hypoxia detection (reproduced with permission from [42]); (b) Schematic of in vivo multimodal imaging system, which is capable of generating US (ultrasound), PAI, and PALI images using the same hardware (reproduced with permission from [45]. Copyright SPIE, 2013); (c) A combined PDT/PALI therapy/imaging system. A common fiber-optic bundle is used to deliver light into the tissue. A 660 nm emitting laser-diode is used for PDT. Open development platform is used for ultrasound multi-channel data acquisition. A 64-element US linear array is used for US, PAI, and PALI imaging operation. A FPGA (field programmable gate array) module is used to synchronized laser firing and signal acquisition. A PC is used as a system controller, data processing, and display (reproduced with permission from [47]. Copyright SPIE, 2014).

Although in the early stage, detecting tissue  $pO_2$  by photoacoustic technology shows great potentials in both research and clinical theranostics. In vivo complexity has made production or transportation study of proteins, ions, or oxygen challenging. Technical development for deep tissue functional imaging is in urgent demand for comprehensive understanding of biological processes. Photoacoustic imaging is entering its translational stage, and expansion of its applications will greatly help promote this progress. Due to the intrinsic fine resolution, real-time imaging ability, deep penetration depth, etc., PAI is highly promising for deep tissue  $pO_2$  measurement. Future work should stress the accuracy, finer resolution, deeper penetration, real-time imaging, and combination with  $sO_2$  monitoring to get the overall knowledge of the region of interest. For example, through wavefront engineering [52], it has potential to achieve whole body detection of oxygen distribution in a real-time and non-invasive way, which is a long-sought goal in both biomedical research and clinics. In addition, works discussed above applying lifetime method exploited specific oxygen-sensitive dyes, which detected triplet oxygen molecules while generating singlet oxygen at the same time. This can act as a double-edged sword, which is bad for normal cells if there is too much of such byproduct, but can be good for theragnostic performance in cancerous cells. In this regard, it is highly preferable to develop oxygen sensitive dyes that have peak absorption in the near infrared region (being suitable for in vivo PAI) yet produce few adverse effects to cells. These kinds of studies can potentially greatly facilitate tissue hypoxia detection, early cancer diagnosis, as well as hyperbaric or radiation therapy.

#### 4. Conclusions

In this review, we combined two biological oxygen-related parameters— $sO_2$  and  $pO_2$ —and their corresponding detection methods. Grand significance is attached to applications of photoacoustic technique in this field. Use of the photoacoustic spectrum combined with preferential absorption of hemoglobin makes it a uniquely effective tool for blood oxygen saturation detection. Meanwhile, photoacoustic imaging also shows great potential in tissue oxygen partial pressure evaluation. Combining these two parameters and integrating them into one single system will significantly advance the extensive understanding of oxygen functions in our body and further progress in cancer diagnosis and therapy.

**Acknowledgments:** The work has been supported by the Hong Kong Research Grant Council (No. 252044/16E) and the National Natural Science Foundation of China (No. 81671726 and No. 81627805).

**Conflicts of Interest:** The authors declare no conflict of interest.

#### References

1. Giaccia, A.J.; Simon, M.C.; Johnson, R. The biology of hypoxia: The role of oxygen sensing in development, normal function, and disease. *Genes Dev.* **2004**, *18*, 2183–2194. [[CrossRef](#)] [[PubMed](#)]
2. Fidler, I.J. Angiogenesis and cancer metastasis. *Cancer J.* **2000**, *6*, S134–S141. [[PubMed](#)]
3. Hockel, M.; Vaupel, P. Tumor Hypoxia: Definitions and Current Clinical, Biologic, and Molecular Aspects. *J. Natl. Cancer Inst.* **2001**, *93*, 266–276. [[CrossRef](#)] [[PubMed](#)]
4. Moen, I.; Stuhr, L.E.B. Hyperbaric oxygen therapy and cancer—A review. *Target. Oncol.* **2012**, *7*, 233–242. [[CrossRef](#)] [[PubMed](#)]
5. Song, G.; Ji, C.; Liang, C.; Song, X.; Yi, X.; Dong, Z.; Yang, K.; Liu, Z. TaOx decorated perfluorocarbon nanodroplets as oxygen reservoirs to overcome tumor hypoxia and enhance cancer radiotherapy. *Biomaterials* **2017**, *112*, 257–263. [[CrossRef](#)] [[PubMed](#)]
6. Littlejohns, L.R.; Bader, M.K.; March, K. Brain Tissue Oxygen Monitoring in Severe Brain Injury, I: Research and Usefulness in Critical Care. *Crit. Care Nurse* **2003**, *23*, 17–25. [[PubMed](#)]
7. Rosenthal, G.; Hemphill, J.C., 3rd; Sonani, M.; Martin, C.; Morabito, D.; Obrist, W.D.; Manley, G.T. Brain tissue oxygen tension is more indicative of oxygen diffusion than oxygen delivery and metabolism in patients with traumatic brain injury. *Crit. Care Med.* **2008**, *36*, 1917–1924. [[CrossRef](#)] [[PubMed](#)]
8. Sheffield, P.J. Measuring tissue oxygen tension: A review. *Undersea Hyperb. Med.* **1998**, *25*, 179–188. [[PubMed](#)]
9. Diaz-Tena, E.; Barona, A.; Gallastegui, G.; López de Lacalle, L.N.; Elías, A. Biomachining: Metal etching via microorganisms. *Crit. Rev. Biotechnol.* **2017**, *37*, 323–332. [[CrossRef](#)] [[PubMed](#)]
10. Díaz-Tena, E.; Gallastegui, G.; Hipperdinger, M.; Donati, E.R.; Ramírez, M.; Rodríguez, A.; López de Lacalle, L.N.; Elías, A. New advances in copper biomachining by iron-oxidizing bacteria. *Corros. Sci.* **2016**, *112*, 385–392. [[CrossRef](#)]
11. Hummler, H.D.; Engelmann, A.; Pohlandt, F.; Högel, J.; Franz, A.R. Accuracy of pulse oximetry readings in an animal model of low perfusion caused by emerging pneumonia and sepsis. *Intensive Care Med.* **2004**, *30*, 709–713. [[CrossRef](#)] [[PubMed](#)]
12. De Santis, V.; Singer, M. Tissue oxygen tension monitoring of organ perfusion: Rationale, methodologies, and literature review. *Br. J. Anaesth.* **2015**, *115*, 357–365. [[CrossRef](#)] [[PubMed](#)]
13. Wang, L.V.; Yao, J. A practical guide to photoacoustic tomography in the life sciences. *Nat. Methods* **2016**, *13*, 627–638. [[CrossRef](#)] [[PubMed](#)]
14. Xu, M.; Wang, L.V. Photoacoustic imaging in biomedicine. *Rev. Sci. Instrum.* **2006**, *77*, 041101. [[CrossRef](#)]
15. Beard, P. Biomedical photoacoustic imaging. *Interface Focus* **2011**, *1*, 602–631. [[CrossRef](#)] [[PubMed](#)]
16. Yao, J.; Wang, L.V. Sensitivity of photoacoustic microscopy. *Photoacoustics* **2014**, *2*, 87–101. [[CrossRef](#)] [[PubMed](#)]
17. Wang, X.; Xie, X.; Ku, G.; Wang, L.V.; Stoica, G. Noninvasive imaging of hemoglobin concentration and oxygenation in the rat brain using high-resolution photoacoustic tomography. *J. Biomed. Opt.* **2006**, *11*, 024015. [[CrossRef](#)] [[PubMed](#)]

18. Zhang, H.F.; Maslov, K.; Sivaramakrishnan, M.; Wang, L.V. Imaging of hemoglobin oxygen saturation variations in single vessels in vivo using photoacoustic microscopy. *Appl. Phys. Lett.* **2007**, *90*, 053901. [[CrossRef](#)]
19. Li, W.; Lin, L.; Li, G. Wavelength selection method based on test analysis of variance: Application to oximetry. *Anal. Methods* **2014**, *6*, 1082–1089. [[CrossRef](#)]
20. Lopez Silva, S.M.; Dotor Castilla, M.L.; Silveira Martin, J.P. Near-infrared transmittance pulse oximetry with laser diodes. *J. Biomed. Opt.* **2003**, *8*, 525–533. [[CrossRef](#)] [[PubMed](#)]
21. Zhang, H.F.; Masloc, K.; Stoica, G.; Wang, L.V. Imaging acute thermal burns by photoacoustic microscopy. *J. Biomed. Opt.* **2006**, *11*, 054033. [[CrossRef](#)] [[PubMed](#)]
22. Yao, J.; Maslov, K.I.; Zhang, Y.; Xia, Y.; Wang, L.V. Label-free oxygen-metabolic photoacoustic microscopy in vivo. *J. Biomed. Opt.* **2011**, *16*, 076003. [[CrossRef](#)] [[PubMed](#)]
23. Ning, B.; Kennedy, M.J.; Dixon, A.J.; Sun, N.; Cao, R.; Soetikno, B.T.; Chen, R.; Zhou, Q.; Kirk Shuang, K.; Hossack, J.A.; et al. Simultaneous photoacoustic microscopy of microvascular anatomy, oxygen saturation, and blood flow. *Opt. Lett.* **2015**, *40*, 910–913. [[CrossRef](#)] [[PubMed](#)]
24. Yao, J.; Wang, L.; Yang, J.M.; Maslov, K.I.; Wong, T.T.; Li, L.; Huang, C.H.; Zou, J.; Wang, L.V. High-speed label-free functional photoacoustic microscopy of mouse brain in action. *Nat. Methods* **2015**, *12*, 407–410. [[CrossRef](#)] [[PubMed](#)]
25. Bayer, C.L.; Wlodarczyk, B.J.; Finnell, R.H.; Emelianov, S.Y. Ultrasound-guided spectral photoacoustic imaging of hemoglobin oxygenation during development. *Biomed. Opt. Express* **2017**, *8*, 757–763. [[CrossRef](#)] [[PubMed](#)]
26. Rich, L.J.; Seshadri, M. Photoacoustic monitoring of tumor and normal tissue response to radiation. *Sci. Rep.* **2016**, *6*, 21237. [[CrossRef](#)] [[PubMed](#)]
27. Dasu, A.; Toma-Dasu, I. Vascular oxygen content and the tissue oxygenation—A theoretical analysis. *Med. Phys.* **2008**, *35*, 539–545. [[CrossRef](#)] [[PubMed](#)]
28. Hockel, M.; Knoop, C.; Schlenger, K.; Vorndran, B.; Baulmann, E.; Mitze, M.; Knapstein, P.G.; Vaupel, P. Intratumoral pO<sub>2</sub> predicts survival in advanced cancer of the uterine cervix. *Radiother. Oncol.* **1993**, *26*, 45–50. [[CrossRef](#)]
29. Cramer, T.; Schmitt, C.A. *Metabolism in Cancer*; Springer International Publishing: Cham, Switzerland, 2016.
30. Lu, F.M.; Yuan, Z. PET/SPECT molecular imaging in clinical neuroscience: Recent advances in the investigation of CNS diseases. *Quant. Imaging Med. Surg.* **2015**, *5*, 433–447. [[PubMed](#)]
31. Krohn, K.A.; Link, J.M.; Mason, R.P. Molecular imaging of hypoxia. *J. Nucl. Med.* **2008**, *49*, 129S–148S. [[CrossRef](#)] [[PubMed](#)]
32. Haris, M.; Yadav, S.K.; Rizwan, A.; Singh, A.; Wang, E.; Hariharan, H.; Reddy, R.; Marincola, F.M. Molecular magnetic resonance imaging in cancer. *J. Trans. Med.* **2015**, *13*, 313–328. [[CrossRef](#)] [[PubMed](#)]
33. Lövblad, K.O.; Anzalone, N.; Dörfler, A.; Essig, M.; Hurwitz, B.; Kappos, L.; Lee, S.K.; Filippi, M. MR Imaging in Multiple Sclerosis: Review and Recommendations for Current Practice. *Am. J. Neuroradiol.* **2010**, *31*, 983–989. [[CrossRef](#)] [[PubMed](#)]
34. Tatum, J.L.; Kelloff, G.J.; Gillies, R.J. Hypoxia: Importance in tumor biology, noninvasive measurement by imaging, and value of its measurement in the management of cancer therapy. *Int. J. Radiat. Biol.* **2006**, *82*, 699–757. [[CrossRef](#)] [[PubMed](#)]
35. Ntziachristos, V. Going deeper than microscopy: The optical imaging frontier in biology. *Nat. Methods* **2010**, *7*, 603–614. [[CrossRef](#)] [[PubMed](#)]
36. Kautsky, H.; Hirsch, A. Original observation of effectdyes absorbed on silica gel. *Z. Anorg. Allg. Chem.* **1935**, *222*, 126–134.
37. Vanderkooi, J.M.; Maniara, G.; Green, T.J.; Wilson, D.F. An Optical Method for Measurement of Dioxygen Concentration Based upon Quenching of Phosphorescence. *J. Biol. Chem.* **1987**, *262*, 5476–5482. [[PubMed](#)]
38. Holst, G.; Grunwald, B. Luminescence lifetime imaging with transparent oxygen optodes. *Sens. Actuators B Chem.* **2001**, *74*, 78–90. [[CrossRef](#)]
39. Becker, W. *Advanced Time Correlated Single Photon Counting Applications*; Springer International Publishing: Cham, Switzerland, 2015.

40. Piffaretti, F.; Novello, A.M.; Kumar, R.S.; Forte, E.; Paulou, C.; Nowak-Sliwinska, P.; van den Bergh, H.; Wagnières, G. Real-time, in vivo measurement of tissular pO<sub>2</sub> through the delayed fluorescence of endogenous protoporphyrin IX during photodynamic therapy. *J. Biomed. Opt.* **2012**, *17*, 115007. [[CrossRef](#)] [[PubMed](#)]
41. Suhling, K.; Hirvonen, L.M.; Levitt, J.A.; Chung, P.H.; Tregidgo, C.; Le Marois, A.; Rusakov, D.A.; Zheng, K.; Ameer-Beg, S.; Poland, S.; et al. Fluorescence lifetime imaging (FLIM): Basic concepts and some recent developments. *Med. Photonics* **2015**, *27*, 3–40. [[CrossRef](#)]
42. Shao, Q. Photoacoustic Lifetime Imaging and Its Biomedical Applications. Ph.D Thesis, University of Minnesota, Minneapolis, MN, USA, January 2016; p. 8.
43. Ashkenazi, S.; Huang, S.W.; Horvath, T.; Koo, Y.E.; Kopelman, R. Photoacoustic probing of fluorophore excited state lifetime with application to oxygen sensing. *J. Biomed. Opt.* **2008**, *13*, 034023. [[CrossRef](#)] [[PubMed](#)]
44. Ashkenazi, S. Photoacoustic lifetime imaging of dissolved oxygen using methylene blue. *J. Biomed. Opt.* **2010**, *15*, 040501. [[CrossRef](#)] [[PubMed](#)]
45. Shao, Q.; Morgounova, E.; Jiang, C.; Choi, J.; Bischof, J.; Ashkenazi, S. In vivo photoacoustic lifetime imaging of tumor hypoxia in small animals. *J. Biomed. Opt.* **2013**, *18*, 076019. [[CrossRef](#)] [[PubMed](#)]
46. Shao, Q.; Ashkenazi, S. Photoacoustic lifetime imaging for direct in vivo tissue oxygen monitoring. *J. Biomed. Opt.* **2015**, *20*, 036004. [[CrossRef](#)] [[PubMed](#)]
47. Shao, Q.; Biel, M.A.; Ashkenazi, S. Noninvasive tumor oxygen imaging by photoacoustic lifetime imaging integrated with photodynamic therapy. *Proc. SPIE* **2014**, *8931*, 89310H.
48. Shao, Q.; Morgounova, E.; Ashkenazi, S. Tissue oxygen monitoring by photoacoustic lifetime imaging (PALI) and its application to image-guided photodynamic therapy (PDT). *Proc. SPIE* **2015**, *9323*, 932320.
49. Ray, A.; Rajian, J.R.; Lee, Y.E.; Wang, X.; Kopelman, R. Lifetime-based photoacoustic oxygen sensing in vivo. *J. Biomed. Opt.* **2012**, *17*, 057004. [[CrossRef](#)] [[PubMed](#)]
50. Raya, A.; Rajian, J.R.; Lee, Y.-E.K.; Wang, X.; Kopelman, R. In vivo oxygen sensing using lifetime based photoacoustic measurements. *Proc. SPIE* **2013**, *8581*, 85811Q.
51. Jo, J.; Lee, C.H.; Kopelman, R.; Wang, X. Lifetime-resolved photoacoustic (LPA) spectroscopy for monitoring oxygen change and photodynamic therapy (PDT). *Proc. SPIE* **2016**, *9708*, 97081L.
52. Lai, P.; Wang, L.; Tay, J.W.; Wang, L.V. Photoacoustically guided wavefront shaping for enhanced optical focusing in scattering media. *Nat. Photonics* **2015**, *9*, 126–132. [[CrossRef](#)] [[PubMed](#)]



© 2017 by the authors. Licensee MDPI, Basel, Switzerland. This article is an open access article distributed under the terms and conditions of the Creative Commons Attribution (CC BY) license (<http://creativecommons.org/licenses/by/4.0/>).